

On the absence of molecular absorption in high-redshift millimetre-band searches

S. J. Curran,^{1*} M. T. Whiting,^{1,2} F. Combes,³ N. Kuno,⁴ P. Francis,⁵ N. Nakai,⁶
J. K. Webb,¹ M. T. Murphy^{1,7} and T. Wiklind^{8,9,10}

¹*School of Physics, University of New South Wales, Sydney, NSW 2052, Australia*

²*CSIRO Australia Telescope National Facility, PO Box 76, Epping, NSW 1710, Australia*

³*LERMA, Observatoire de Paris, 77 Avenue Denfert-Rochereau, 75014 Paris, France*

⁴*Nobeyama Radio Observatory, Nagano 384-1305, Japan*

⁵*Australian National University, Canberra, Australia*

⁶*Institute of Physics, University of Tsukuba, Ten-noudai, Tsukuba, Ibaraki 305-8571, Japan*

⁷*Centre for Astrophysics and Supercomputing, Swinburne University of Technology, PO Box 218, Hawthorn, VIC 3122, Australia*

⁸*Space Telescope Science Institute, Baltimore, MD 21218, USA*

⁹*Onsala Space Observatory, S-439 92 Onsala, Sweden*

¹⁰*Joint ALMA Observatory, Santiago, Chile*

Accepted 2011 June 3. Received 2011 June 3; in original form 2011 March 31

ABSTRACT

We have undertaken a search for millimetre-waveband absorption (through the CO and HCO⁺ rotational transitions) in the host galaxies of reddened radio sources ($z = 0.405\text{--}1.802$). Despite the colour selection (optical–near-infrared colours of $V - K \gtrsim 5$ in all but one source), no absorption was found in any of the eight quasars for which the background continuum flux was detected. On the basis of the previous (mostly intervening) H₂ and OH detections, the limits reached here and in some previous surveys should be deep enough to detect molecular absorption according to their $V - K$ colours. However, our survey makes the assumption that the reddening is associated with dust close to the emission redshift of the quasar and that the narrow millimetre component of this emission is intercepted by the compact molecular cores. By using the known millimetre absorbers to define the *colour depth* and comparing this with the ultraviolet luminosities of the sources, we find that, even if these assumptions are valid, only 12 of the 40 objects (mainly from this work) are potentially detectable. This is assuming an excitation temperature of $T_x = 10$ K at $z = 0$, with the number decreasing with increasing temperatures (to zero detectable at $T_x \gtrsim 100$ K).

Key words: galaxies: abundances – galaxies: active – galaxies: high-redshift – quasars: absorption lines – cosmology: observations – radio lines: galaxies.

1 INTRODUCTION

Millimetre-wave observations of molecular absorption systems along the sightlines to distant quasars provide a powerful probe of the cold, dense, star-forming gas in the distant Universe. Furthermore, a comparison of the redshifts of the rotational transitions of the molecules with those of the spin-flip transition of H I, as well as the electronic optical/UV transitions of metal ions, can be used to determine high-redshift values of the fundamental constants, to at least an order of magnitude the sensitivity of purely optical data (see Curran, Kanekar & Darling 2004a). However, despite much searching, only four such systems are

currently known (Wiklind & Combes 1995; 1996a; 1997), the highest redshift being at $z_{\text{abs}} = 0.89$. Of these, two are intervening systems (gravitational lenses towards more distant quasars), with the other two systems arising through absorption within the host galaxy of the quasar. Subsequent searches at the redshifts of known high column density H I absorption systems, intervening the sightlines to more distant quasi-stellar objects (QSOs), have also failed to detect molecular absorption in the millimetre-band (Curran et al. 2004b and references therein), despite the possibility that these so-called damped Lyman α systems (DLAs)¹

¹ These have neutral hydrogen column densities of $N_{\text{H I}} \geq 2 \times 10^{20} \text{ cm}^{-2}$ and are usually detected at $z_{\text{abs}} \gtrsim 1.8$, where the Lyman α transition is redshifted into the optical band.

*E-mail: sjc@phys.unsw.edu.au

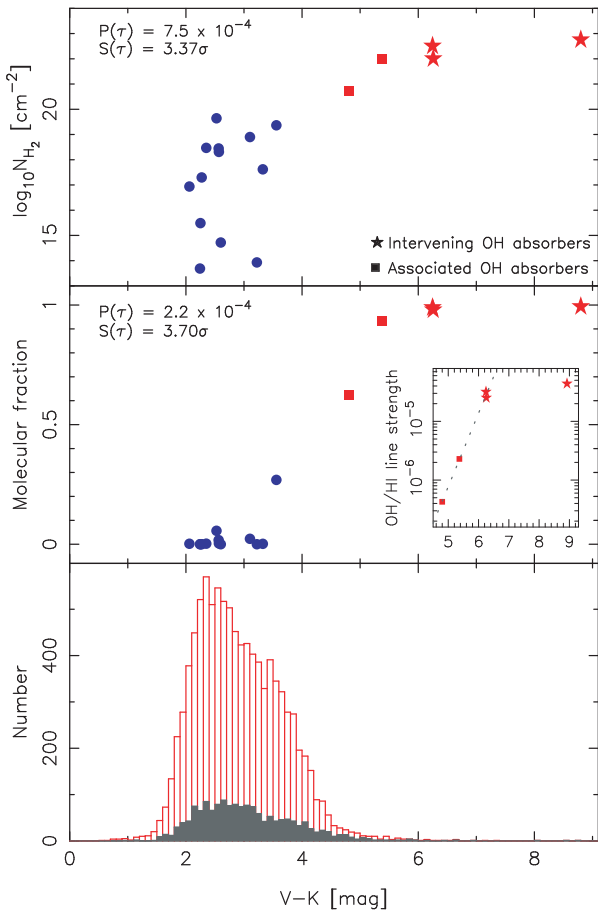


Figure 1. The H_2 column density (top) and the molecular fraction (middle) versus the observed frame optical–near-infrared colour (where available) for high-redshift molecular absorption systems. The circles represent the H_2 -bearing DLAs (all optically selected intervening absorbers) and the squares and stars represent the OH absorbers (radio selected), with the inset in the middle panel showing the normalized OH line strength (Curran et al. 2006). These are comprised of the four systems originally identified in millimetre-wave transitions (with the least-squares fit to these shown) plus the gravitational lens at $z_{\text{abs}} = 0.764$ towards 0132–097 (detected in OH decimetre but not HCO^+ millimetre absorption, Kanekar et al. 2005). $P(\tau)$ shows Kendall’s τ two-sided probability of the observed distribution occurring by chance and $S(\tau)$ the significance of this assuming Gaussian statistics. The bottom panel shows the distribution of SDSS quasars (Schneider et al. 2007, after conversion to V magnitudes, Fukugita et al. 1996) where the filled histogram shows those which have been detected in the Very Large Array’s ‘Faint Images of the Radio Sky at Twenty Centimetres’ (FIRST) survey (Becker, White & Helfand 1995).

may account for more than 80 per cent of the neutral gas content in the Universe (Prochaska, Herbert-Fort & Wolfe 2005).

DLAs are, however, not devoid of molecular gas: to date, the Lyman and Werner ultraviolet bands of H_2 have been detected in 19 DLAs (see Noterdaeme et al. 2008;² Jorgenson et al. 2009; Srianand et al. 2010). These, however, have molecular abundances which are generally much lower than those detectable with current microwave and radio telescopes (Curran et al. 2004b and Fig. 1, top). Furthermore, in Curran et al. (2006) we showed that the H_2 -bearing DLAs have molecular fractions of $\mathcal{F} \equiv \frac{2N_{\text{H}_2}}{2N_{\text{H}_2} + N_{\text{HI}}} \sim$

² One of which, J1439 + 113, has also been detected in the CO $A - X$ UV band (Srianand et al. 2008).

10^{-7} –0.3 and $V - K \lesssim 4$ (Fig. 1, middle), i.e. in the same range as a ‘typical’ QSO (Fig. 1, bottom),³ whereas the millimetre- and decimetre-band absorbers have molecular fractions of $\mathcal{F} \approx 0.6$ –1 and optical–near-infrared colours of $V - K \gtrsim 5$.

The correlations in Fig. 1 present strong evidence that the quasar light is reddened by dust in the foreground absorber: since the presence of the dust is necessary to prevent the dissociation of the molecular gas by the ambient ultraviolet field, the molecular fraction is expected to be correlated with the dust abundance, as observed. The paucity of millimetre-waveband absorption can therefore be attributed to the traditional optical selection of targets biasing towards absorbers of low dust content and therefore low molecular fractions.

The fact that intervening absorbers are usually found through optical spectroscopy, yielding a redshift but also giving the above bias against dusty objects, means that millimetre-band searches of known intervening absorbers have generally been unsuccessful (Curran et al. 2004b and references therein). An alternative target for molecular absorption is towards the fainter ‘red quasars’, where the red colour may indicate an intervening column of dust. However, due to the relatively narrow bandwidths in the millimetre band (see Section 4.2), such an approach is currently only practical at longer (decimetre) wavelengths (see Curran et al. 2011b). In the absence of any known intervening absorbers, selecting the quasar itself gives a redshift (z_{em}) to which to tune the receiver. Naturally, such a selection of targets prevents any useful comparison with the optical redshifts, in order to measure the values of the fundamental constants, although any detections could be followed up in 21 cm, giving the redshift of the spin-flip transition of H I.

In Curran et al. (2006, 2008, 2011a), we presented the results from our decimetre-wave searches for such ‘associated’ (OH and H I) absorption and here we present the results of our millimetre-wave survey for the associated absorption.

2 OBSERVATIONS

2.1 Target selection

As per Curran et al. (2006), our sources were selected from the Parkes Half-Jansky Flat-spectrum Sample (PHFS, Drinkwater et al. 1997),⁴ on the basis of their optical–near-IR photometry (Francis, Whiting & Webster 2000). From these, we selected the 30 reddest sources (which correspond to an extinction of $A_V \approx 4.1$), in which the emission redshift of the quasar (z_{em}) would place a strong absorption line (CO or HCO^+) into the 3-mm band. After culling these further, by selecting those of $\delta > -30^\circ$ (thus being observable from northern latitudes)⁵ and with 3-mm flux densities expected to be $\gtrsim 100$ mJy, the 10 objects listed in Table 1 remained.

2.2 The IRAM 30-m observations

From 2003 December to 2004 February we observed three of the targets with the IRAM (Institut de Radio Astronomie Millimétrique) 30-m telescope at Pico Veleta, Spain. We used two

³ $V - K = 2.88 \pm 1.04$ in general and 3.05 ± 0.97 if radio-loud.

⁴ With the addition of 0500 + 019, included since it has been detected in 21-cm absorption (Carilli et al. 1998). We also included J0906 + 4952 and J1341 + 3301, which are two very red sources from Glikman et al. (2004) (Section 2.3).

⁵ We miss SEST.

Table 1. The search results. $V - K$ is the optical–near-infrared colour (see Curran et al. 2006, 2008 and references therein, and Glikman et al. 2004); z_{em} is the emission redshift of the target; ‘Tel.’ gives the telescope used with the total integration time in hours, t_{int} , followed by the transition searched along with the central tuned frequency (GHz); σ_{rms} is the rms noise (mK) reached per Δv channel (km s^{-1}); and T_{cont} is the continuum measured in T_{A}^* (mK). This is converted to a flux density S_{cont} (Jy), using a conversion of 6 Jy K^{-1} for the IRAM 30-m at 3-mm and $\eta_{\text{mb}} = 0.79$ (32 GHz), 0.77 (43 GHz), 0.51 (86 GHz) and 0.52 (100 GHz) for the NRO 45 m. $\tau = -\ln(1 - 3\sigma_{\text{rms}}/T_{\text{cont}})$ is the optical depth limit of the relevant millimetre line calculated from the rms noise per estimated FWHM, except for 0454 + 066 and J1341 + 3301, which are 2 and 70 km s^{-1} , respectively (see main text). N_{total} (cm^{-2}) is the total column density per channel of the relevant molecule obtained from this (for an excitation temperature of $T_x = 10 \text{ K}$ at $z = 0$; see the main text) over the redshift range quoted.

Source	$V - K$	z_{em}	Tel.	t_{int}	Transition	ν_{obs}	σ_{rms}	Δv	T_{cont}	S_{cont}	τ (3σ)	N_{total}	z range
0213 – 026	5.65	1.178	NRO	10.4	$\text{HCO}^+ 0 \rightarrow 1$	40.95	5.9	0.9	91	0.24	<0.058	$<7.8 \times 10^{12}$	1.1712–1.1848
...	NRO	2.0	$\text{CO } 1 \rightarrow 2$	105.85	12	0.37	33	0.13	<0.23	$<1.1 \times 10^{16}$	1.1754–1.1806
0454 + 066	4.32	0.405	NRO	5.0	$\text{CO } 0 \rightarrow 1$	82.04	10	0.45	120	0.48	<0.13	$<1.8 \times 10^{15}$	0.4028–0.4072
0500 + 019	5.75	0.584 57*	IRAM	12.8	$\text{HCO}^+ 1 \rightarrow 2$	112.57	1.6	3.4	23	0.14	<0.11	$<6.3 \times 10^{12}$	0.5811–0.5882
J0906 + 4952	5.68	1.635	NRO	2.2	$\text{HCO}^+ 0 \rightarrow 1$	33.85	12	1.1	<12	<0.03	–	–	1.6251–1.6450
1107 – 187	5.15	0.497	NRO	3.7	$\text{CO } 0 \rightarrow 1$	77.00	16	0.51	54	0.21	<0.38	$<1.1 \times 10^{16}$	0.4945–0.4995
J1341 + 3301	7.19	1.720	NRO	1.1	$\text{HCO}^+ 0 \rightarrow 1$	32.79	25	1.1	550	1.41	<0.017	$<1.8 \times 10^{13}$	1.7094–1.7307
1430–155	5.74	1.573	IRAM	13.6	$\text{CO } 1 \rightarrow 2$	89.60	1.0	4.2	31	0.18	<0.057	$<3.5 \times 10^{15}$	1.5658–1.5802
1504–166	5.74	0.876	IRAM	7.2	$\text{HCO}^+ 1 \rightarrow 2$	95.08	1.9	3.9	126	0.76	<0.025	$<1.5 \times 10^{12}$	0.8711–0.8810
1706 + 006	4.96	0.449	NRO	8.5	$\text{CO } 0 \rightarrow 1$	79.55	7.8	0.48	–	–	–	–	0.4467–0.4513
2337 – 334	5.50	1.802	NRO	12.9	$\text{HCO}^+ 0 \rightarrow 1$	31.83	4.4	1.2	113	0.29	<0.045	$<2.9 \times 10^{12}$	1.7908–1.8133

*The mean redshift of the H I 21-cm absorption detected by Carilli et al. (1998) which has two components, giving a total column density of $N_{\text{HI}} = 6.2 \times 10^{18} (T_s/f) \text{ cm}^{-2}$.

3-mm superconductor–insulator–superconductor (SIS) receivers (A100 and B100), tuned to the redshifted frequencies of the molecular transitions (see Table 1). The observations were made with a nutating subreflector, switching symmetrically ± 90 arcsec in azimuth with a frequency of 0.5 Hz. The continuum levels of the observed sources were determined using a continuum backend and increasing the subreflector switch frequency to 2 Hz. The image sideband rejection of the receivers were high, of the order of 20 dB (single sideband). System temperatures typically ranged from 120 K (90 GHz) to 180 K (113 GHz). We used the full 1-GHz backend with broad (1 MHz) filter banks and narrow-band autocorrelators, the former giving a channel spacing of $\approx 3\text{--}4 \text{ km s}^{-1}$ (Table 1) over a bandwidth of $\approx 1500 \text{ km s}^{-1}$, which should be sufficient to cover uncertainties in the emission redshifts, all of which are known to at least three decimal places ($\Delta z = \pm 0.001$ corresponds to $\Delta v \approx \pm 100\text{--}200 \text{ km s}^{-1}$ for our sample). The pointing of the telescope was checked regularly on nearby continuum sources. Typical pointing corrections were 5–10 arcsec. The focus was checked regularly on Mars and Saturn. The half power beam width (HPBW) at 95 GHz is 26 arcsec.

We prioritized the three targets according to the 3-mm flux densities estimated from an interpolation of the decimetre and near-infrared values: 12.8 h of integration on 0500 + 019 ($S_{\text{est}} \approx 0.32 \text{ Jy}$), 13.6 h on 1430–155 ($S_{\text{est}} \gtrsim 0.08 \text{ Jy}$) and 7.2 h on 1504–166 ($S_{\text{est}} \gtrsim 0.8 \text{ Jy}$), which, upon comparison with the observed values (Table 1), were reasonable estimates. The data were reduced with the GILDAS⁶ software package.

2.3 The NRO 45-m observations

The remainder of the sample was observed with the Nobeyama Radio Observatory’s 45-m telescope in 2004 March. We used the H28/32 (1-cm) and the S80, S100 (3-mm) receivers to observe the $J = 0 \rightarrow 1$ and $1 \rightarrow 2$ transitions over a range of redshifts (Table 1). The observations were performed in the position-switching mode, with an integration time of 20 s for each scan. The antenna temperature, T_{A}^* , was obtained by the chopper-wheel method, which

corrected for atmospheric and ohmic losses. System temperatures typically ranged from 200 K (1-cm) to 500 K (3-mm). We used the AOS backend over a 250-MHz split over 2048 channels, which gave channel spacings of 0.37 (3-mm) to 1.1 km s^{-1} (1-cm) with bandwidths of ≈ 700 and $\approx 2000 \text{ km s}^{-1}$, respectively. The pointing of the telescope was checked by observing SiO maser sources with the H40 (40-GHz band) receiver and the corrections were ≤ 10 arcsec.

The 3-mm observations were performed when the weather was clearest, with total integration times of 2 h for 0213–026, 5 h for 0454 + 066, 3.7 h for 1107–187 and 8.5 h for 1706 + 006 (for which we could not determine the flux density, Fig. 2).⁷ During less than ideal weather conditions, we observed in the 1-cm band and included the radio-detected, optically dim sources of Glikman et al. (2004), where $\text{HCO}^+ 0 \rightarrow 1$ is redshifted into this band – the FIRST–2MASS reddened quasars J0906 + 4952 (SDSS J090651.49 + 495235.9) and FTM J1341 + 3301. The data were reduced with the NEWSTAR package and, like the IRAM results, upon the removal of a low-order baseline and smoothing no absorption features were apparent in the spectra.

3 RESULTS

3.1 Observational results

In Fig. 2 we show the reduced spectra and in Table 1 we summarize our observational results. The limit to the total column density of each molecule is calculated from

$$N_{\text{total}} = \frac{8\pi}{c^3} \frac{\nu^3}{g_{J+1} A_{J+1 \rightarrow J}} \frac{Q e^{E_J/kT_x}}{1 - e^{-h\nu/kT_x}} \int \tau dv, \quad (1)$$

where ν is the rest frequency of the $J \rightarrow J + 1$ transition; g_{J+1} and $A_{J+1 \rightarrow J}$ are the statistical weight and the Einstein A-coefficient of the transition, respectively; and $Q = \sum_{J=0}^{\infty} g_J e^{-E_J/kT_x}$ is the

⁷ The highest frequency flux measurement available for 1706 + 006 is 0.44 Jy at 5.0 GHz (Wright & Otrupcek 1990).

⁶ <http://www.iram.fr/IRAMFR/GILDAS/>

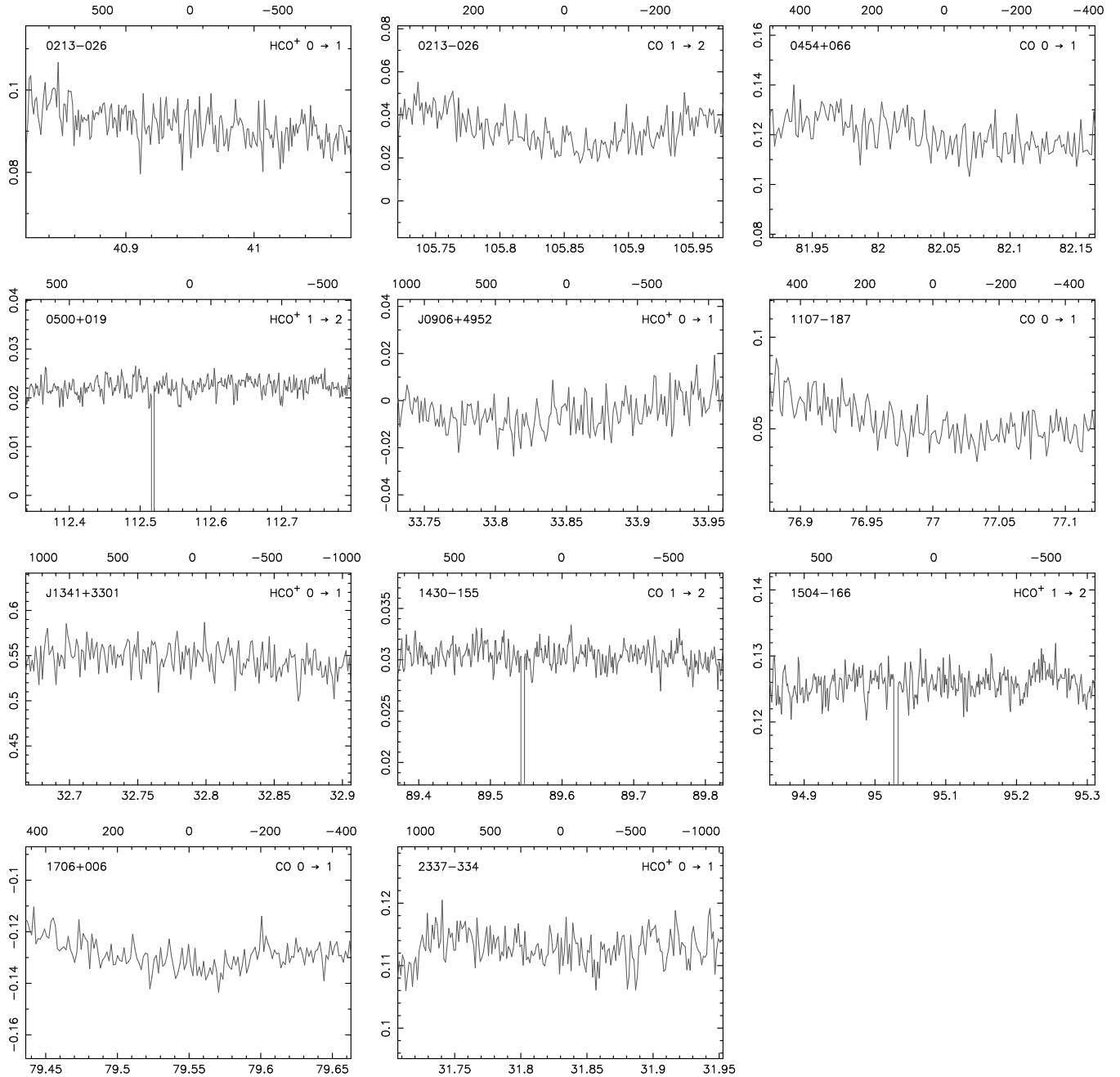


Figure 2. The observed spectra before baseline removal. The ordinate in each spectrum shows the antenna temperature in T_A^* (K) and the abscissa the barycentric frequency (GHz), with the top axis showing the velocity offset from the central tuned frequency (km s^{-1}). All are shown at a resolution of 4 km s^{-1} , the coarsest of the observations (see Table 1). The negative spike in each of the IRAM spectra is due to bad channels (246–250) and the negative flux for 1706 + 006 is due to the long (20 s) integrations with the NRO giving errors in the continuum flux measurement.

partition function.⁸ In the case of the four known systems, the covering factor is expected to be close to unity (Wiklind & Combes 1994, 1995, 1996b, 1998) so, as in the optically thin regime, this can

⁸ The Einstein A-coefficients are taken from Chandra et al. (1995), Chandra, Maheshwari & Sharma (1996) or derived from the permanent electric dipole moment of the molecule, obtained from the JPL Spectral Line Catalog (Pickett et al. 1998), along with the energy of each level, E_J . An online column density calculator based on equation (1) is available from <http://www.phys.unsw.edu.au/~sjc/column/>

be written outside of the integral. However, unlike lower frequency searches (e.g. OH 18-cm, $^2\Pi_{3/2}$), in the millimetre regime even low excitation temperatures give $kT_x \sim E_J \sim h\nu$ and so the column density cannot be approximated via a linear dependence on this. Therefore, unlike the decimetre searches for the associated absorption (Curran et al. 2006, 2008, 2011a), we must assume an excitation temperature.

In Table 2 we apply equation (1) to the velocity-integrated optical depths given in the references in order to derive the column densities and excitation temperatures of the four known systems.

Table 2. The excitation temperatures and column densities derived from the listed references. In the case where the T_x entry is empty, the column density is calculated at the excitation temperature of the other molecule.

System	z_{abs}	Reference	CO		HCO ⁺	
			T_x (K)	N_{total} (cm ⁻²)	T_x (K)	N_{total} (cm ⁻²)
0218 + 357	0.68466	Wiklind & Combes (1995)	9	$6.3 \pm 0.3 \times 10^{16}$	–	$5.1 \pm 0.2 \times 10^{13}$
1413 + 135	0.24671	Wiklind & Combes (1997)	–	$1.54 \pm 0.04 \times 10^{16}$	8	$2.4 \pm 0.4 \times 10^{13}$
1504 + 377	0.67335	Wiklind & Combes (1996b)	16	$5.9 \pm 1.0 \times 10^{16}$	13	$6.5 \pm 0.1 \times 10^{13}$
1830 – 211	0.88582	Wiklind & Combes (1996a, 1998)	–	$\approx 6 \times 10^{17}$	8	$2.9 \pm 0.3 \times 10^{14}$

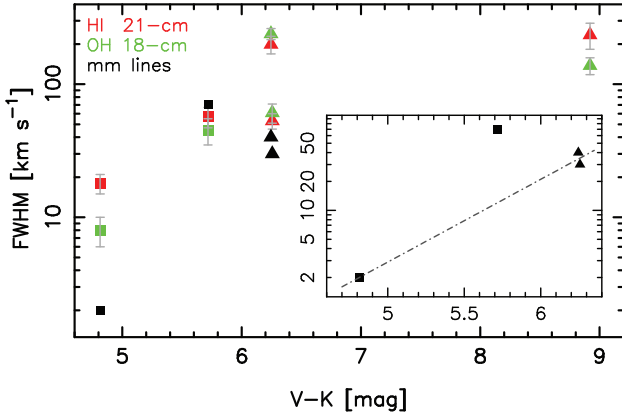


Figure 3. The FWHM of the H I and OH profiles versus the optical–near-infrared colour for the five OH absorbers. The black symbols show the approximate millimetre FWHM versus the optical–near-infrared colour, for the four of the five detected in millimetre lines. The inset shows the millimetre detections only with the line showing the fit used to estimate the FWHM for our targets.

These are found to be close to those derived by Wiklind & Combes (1995, 1996a, b, 1997) and so for our targets we adopt an excitation temperature of $T_x = 10$ K at $z = 0$.

Although the excitation temperatures are similar, the four known millimetre absorbers exhibit a range of full width at half-maxima (FWHMs), ranging from $\text{FWHM} \approx 2 \text{ km s}^{-1}$ (1413 + 135, Wiklind & Combes 1997) to $\approx 70 \text{ km s}^{-1}$ (the main component towards 1504 + 377, Wiklind & Combes 1996b). For these, plus the absorber towards 0132–097 (Section 1), it has been shown that the OH 18-cm ($^2\Pi_{3/2}J = 3/2$) FWHMs are similar to those of the H I 21-cm profiles (Curran et al. 2007), although we cannot yet unambiguously state that millimetre widths are correlated with those of the decimetre lines (Fig. 3). In any case, of all our targets, only one (0500 + 019) has been detected in the 21-cm absorption (see table 6 of Curran et al. 2008 and Section 4.2 of this paper), and so we would have no information on what the width of each of the undetected lines should be. If this were known, we would smooth the spectral resolution (Δv) of the data to the FWHM of the line, thus giving the best possible optical depth limit, based upon the detection of absorption in a single channel. Multiplying the resulting optical depth, scales the velocity integrated optical depth to $\tau \times \text{FWHM}/\Delta v$, giving an overall scaling of $\sqrt{\text{FWHM}/\Delta v}$.

Choosing either the minimum or the maximum FWHM of the four known absorbers therefore gives a possible range in scaling factors of $\sqrt{70/2} \approx 6$, and so the choice of either $\text{FWHM} \approx 2 \text{ km s}^{-1}$ or $\approx 70 \text{ km s}^{-1}$ could lead to a significant over-/underestimate in the profile width. We therefore use the optical–near-infrared colour, which appears to be correlated with the profile width in the four

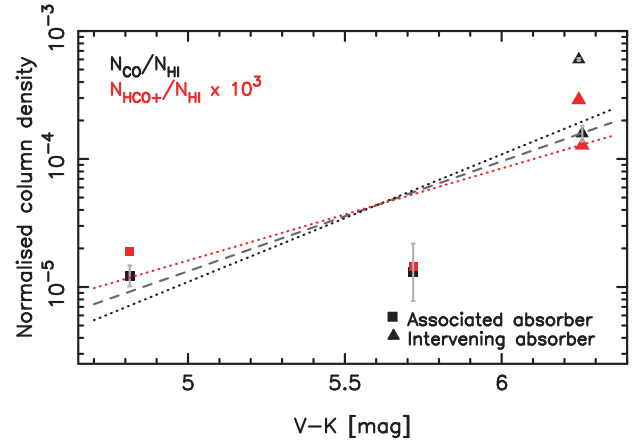


Figure 4. The normalized (assuming $T_x/f = 100$ K) CO (black) and HCO⁺ (coloured) column densities versus optical–near-IR colour. The dotted lines show the least-squares fit for each of the molecules with the dashed line showing the composite fit.

known systems (Fig. 3),⁹ in order to estimate what the FWHM of an undetected absorber should be.

As seen from the figure, the associated absorber in 1504 + 377 represents a stray point with an FWHM of $\approx 70 \text{ km s}^{-1}$. We therefore estimate the profile widths from the least-squares fit to the other three systems (shown in the inset of Fig. 3). The fact that this is based upon only three points, with the removal of one that we simply do not like, limits the robustness of this method, although it should give a better handle on the profile width than a simple assumption. We therefore use this fit, $\log_{10} \text{FWHM} \approx 0.86(V - K) - 3.84$ (for $2 \leq \text{FWHM} \leq 70 \text{ km s}^{-1}$), to estimate the column density limits (given in Table 1).¹⁰

3.2 Comparisons with the known high-redshift molecular absorbers

In Fig. 4 we show the CO and HCO⁺ column densities normalized by that of the H I 21-cm (from Carilli, Perlmán & Stocke 1992; Carilli, Rupen & Yanny 1993; Carilli et al. 1998; Chengalur, de Bruyn & Narasimha 1999) against the optical–near-IR colour, for the four known millimetre absorbers. From this it is difficult to

⁹ This suggests that the path-length through the dust responsible for the reddening may be correlated with the orientation of a rotating cloud complex, such as the disc of a galaxy (Curran & Whiting, in preparation). There is a 1 per cent probability of this correlation arising by chance (for H I, Fig. 3), i.e. a 3.30σ significance assuming Gaussian statistics.

¹⁰ In order to guard against overcompensating, we use the minimum and maximum observed profile widths of 2 and 70 km s^{-1} in cases where the estimated FWHMs are smaller or greater than these limiting values.

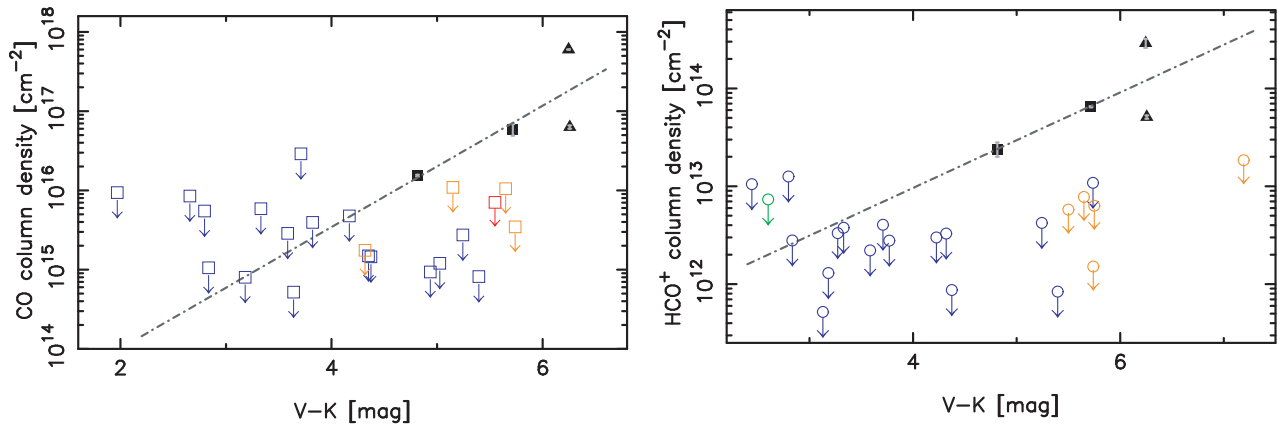


Figure 5. The CO (left) and HCO⁺ (right) column densities versus optical–near-IR colour. The symbols are as per Fig. 4, with the filled symbols showing the four known systems (the line shows the least-squares fit to these) and the unfilled symbols showing the limits from the searches by Wiklind & Combes (1995, 1996b); Drinkwater et al. (1996) (blue) Murphy et al. (2003) (specifically 0727–115 at $z_{\text{em}} = 1.591$, see Section 4.2) and the millimetre-wave searches of Curran et al. (2006) (green) (actually HCN in 0335–122, since this is the only source for which V and K are available) and this paper (orange). All of the limits are at the 3σ level per channel recalculated for the expected FWHM, except when outside the range of the four known, where either 2 or 70 km s⁻¹ is used (Section 3.1). Note that this range may add a potential uncertainty of 0.78 dex to the column density estimates (Section 3.1, although see footnotes 12 and 13), in addition to further uncertainty from the assumption of $T_x = 10$ K at $z = 0$ (see Section 4.3).

ascertain whether there is a correlation between the normalized millimetre-wave column density and the $V - K$ colour, as is found for the normalized OH column densities in Curran et al. (2006) (Fig. 1). Furthermore, 21-cm line strengths are not available for the sample although in Curran et al. (2006) there was still a, albeit more scattered, correlation between the unnormalized OH $^2\Pi_{3/2}$ $J = 3/2$ column density and the $V - K$ colour, which appears to apply to all of the molecular absorbers (Fig. 1, top). Therefore in Fig. 5 we show the unnormalized CO and HCO⁺ column densities against the colour for our targets, as well as those from previous searches of associated molecular absorption (Wiklind & Combes 1995, 1996b; Drinkwater, Combes & Wiklind 1996; Murphy, Curran & Webb 2003; Curran et al. 2008).¹¹

From these, we see that many of the limits (especially the new ones reported in this paper, shown in orange), should be more than sufficient to detect molecular absorption, particularly HCO⁺. Incorporating the upper limits of the column densities, via the ASURV survival analysis package (Isobe, Feigelson & Nelson 1986), gives Kendall’s τ two-sided probabilities of $P(\tau) = 0.0092$ ($n = 26$) [i.e. a significance of $S(\tau) = 2.60\sigma$ for CO]¹² and $P(\tau) = 0.025$ ($n = 27$) [$S(\tau) = 2.24\sigma$ for HCO⁺]¹³ of the column density–colour correlations occurring by chance. For the five known OH absorbers, $S(\tau) = 1.96\sigma$ (Curran et al. 2011a), which falls to 1.36σ for those four detected in millimetre transitions.¹⁴ So although the search results do not lessen the significance of the column density–colour correlations (but actually increase them), many of the limits are be-

low those expected of a detection and so we discuss other possible reasons as to why millimetre-wave spectral lines went undetected in this study and in the previous surveys.

4 DISCUSSION: POSSIBLE EXPLANATIONS FOR THESE AND THE PREVIOUS NON-DETECTIONS

4.1 Millimetre-wave covering factors

While there is an apparent correlation between the normalized column density and the optical–near-infrared colour, Fig. 1 actually shows the ratio of the OH 18-cm velocity-integrated optical depth to that of the H I 21-cm. Therefore in order for the fit to be accurate for the normalized column densities, the four known millimetre absorbers must also have similar spin and excitation temperatures, as well as H I and OH covering factors (or at least a similar ratio of these quantities). While the excitation temperatures can be well constrained from the millimetre transitions (Table 2) and the spin temperatures can be removed by not normalizing the column densities (Fig. 4, cf. 5), the covering factor, f , is ingrained into the optical depth via $\tau = -\ln(1 - \frac{\sigma}{fS})$. Since the CO and HCO⁺ lines are optically thick in the four known systems, $-\ln(1 - \frac{\sigma}{fS}) \neq \frac{\sigma}{fS}$, thus not allowing f to be taken out of the integral in equation (1), although, as noted in Section 3.1, if $f \approx 1$ this would have little effect.

In any case, the correlation shown in Fig. 4 does not hold for *all five* of the absorbers: Towards the $z_{\text{em}} = 2.215$ quasar PMN J0134–0931 (0132–097), Kanekar et al. (2005) detected OH at a column density of $N_{\text{OH}} = 5.6 \times 10^{14} (T_x/f)$ cm⁻² in the intervening $z_{\text{abs}} = 0.765$ gravitational lens, although HCO⁺ 1 → 2 was undetected to $\tau < 0.07$. This gives a column density ratio of $N_{\text{OH}} \gtrsim 5600 N_{\text{HCO}^+}$. Curran et al. (2007) have suggested that the non-detection of millimetre absorption towards 0132–097 could be a geometrical effect, where a molecular cloud has a much larger chance of occulting the lower frequencies, since the decimetre emission region is likely to be much larger than the millimetre region (as may also be exhibited by the wider decimetre profiles, Fig. 3). That is, the narrower

¹¹ In the plots we give Wiklind & Combes (1995, 1996b) and Drinkwater et al. (1996) the same colour of symbol as the latter paper includes some of the results of the first two.

¹² Bearing in mind that these limits are subject to the FWHM estimates (Section 3.1), we have also derived the probabilities when applying the two FWHM extrema of the detected absorbers, 2 and 70 km s⁻¹. Not generally being as red as the detected sample, the values do not change for FWHM = 2 km s⁻¹, and for 70 km s⁻¹, $P(\tau)_{70} = 0.0075$ and $S(\tau)_{70} = 2.68\sigma$ ($n = 28$).

¹³ Again, applying FWHM=2 km s⁻¹ introduces no change to the correlation and $P(\tau)_{70} = 0.022$ & $S(\tau)_{70} = 2.29\sigma$ ($n = 30$).

¹⁴ $S(\tau) = 2.25\sigma$ for the five known OH absorbers plus the OH limits (Curran et al. 2011a).

Table 3. Summary of the millimetre-band scans towards 0500 + 019 with the Swedish ESO-Submillimetre Telescope (Murphy et al. 2003) in the order of increasing frequency bands, as tabulated in Curran et al. (2005). We also show the results for 0727 – 155 since the emission redshift, z_{em} , of the quasar is covered (by CO 1 \rightarrow 2, where we show the fractional redshift range based upon $z = 1.547\text{--}1.591$). This is therefore included in our analysis (Fig. 5). The column density limits are calculated from the quoted optical depths per a 18 km s^{-1} (0500 + 019) and 70 km s^{-1} (0727 – 115) channel (Section 3.1), with $T_x = 10 \text{ K}$ at $z = 0$.

Quasar	V	z_{em}	HCO ⁺				CO			
			Trans.	z -range	$\Delta z/z_{\text{em}}$	$N_{\text{total}} (\text{cm}^{-2})$	Trans.	z -range	$\Delta z/z_{\text{em}}$	$N_{\text{total}} (\text{cm}^{-2})$
0500 + 019	21.2	0.58457	0 \rightarrow 1	0.1025–0.1391	0.063	$<4.1 \times 10^{13}$	0 \rightarrow 1	0.4249–0.4722	0.081	$<3.0 \times 10^{16}$
...	0 \rightarrow 1	0.0311–0.0431	0.021	$<2.3 \times 10^{13}$	0 \rightarrow 1	0.3326–0.3482	0.027	$<1.7 \times 10^{16}$
...	1 \rightarrow 2	0.5771–0.5846	0.013	$<1.0 \times 10^{13}$	0 \rightarrow 1	0.0192–0.0283	0.016	$<1.7 \times 10^{16}$
...	1 \rightarrow 2	0.2615–0.3721	0.189	$<1.2 \times 10^{13}$	–	–	–	–
0727 – 115	22.5	1.591	0 \rightarrow 1	0.1025–0.1391	0.023	$<4.3 \times 10^{13}$	0 \rightarrow 1	0.4249–0.4722	0.030	$<3.2 \times 10^{16}$
...	1 \rightarrow 2	1.2049–1.2781	0.046	$<1.7 \times 10^{13}$	–	–	–	–
...	0 \rightarrow 1	0–0.0630	0.040	$<2.1 \times 10^{13}$	0 \rightarrow 1	0.2737–0.3739	0.063	$<1.6 \times 10^{16}$
...	1 \rightarrow 2	0.9710–1.1260	0.097	$<8.5 \times 10^{12}$	1 \rightarrow 2	1.5474–1.7478	0.027	$<7.1 \times 10^{15}$
...	1 \rightarrow 2	0.2615–0.2926	0.020	$<1.7 \times 10^{13}$	1 \rightarrow 2	0.6304–0.6706	0.025	$<1.5 \times 10^{16}$
...	2 \rightarrow 3	0.8922–0.9388	0.029	$<1.7 \times 10^{13}$	2 \rightarrow 3	1.4455–1.5058	0.038	$<1.8 \times 10^{16}$
...	3 \rightarrow 4	1.5229–1.5850	0.039	$<2.9 \times 10^{13}$	–	–	–	–
...	1 \rightarrow 2	0.2004–0.2491	0.031	$<1.5 \times 10^{13}$	1 \rightarrow 2	0.5514–0.6144	0.040	$<1.3 \times 10^{16}$
...	2 \rightarrow 3	0.8005–0.8737	0.046	$<1.4 \times 10^{13}$	2 \rightarrow 3	1.3270–1.4215	0.059	$<1.5 \times 10^{16}$
...	3 \rightarrow 4	1.4006–1.4981	0.061	$<2.5 \times 10^{13}$	–	–	–	–

millimetre emission is less likely to intercept the CO and HCO⁺ gas which will be localized in dense molecular cores. The fact that the millimetre and decimetre emission, and thus absorption, trace different components of the gas could be responsible for the significance of the correlation with colour not changing when normalizing the millimetre column densities by that of the H I (Section 3.2).

In the case of 0132–097, the possibility that the core of the absorbing molecular gas is offset from the centre of the emission may also result in a reduction of the decimetre covering factor, which could be the cause of the normalized OH line strength in 0132–097 not being as high as expected of its colour (i.e. below the fit defined by the others in Fig. 1, right), although more absorbers would be required to verify this.

4.2 Location of the absorbing gas

From the fact that, of our sample, H I has only been detected in 0500 + 019 we may be incorrect in our assumption that the host galaxy is generally the location of the quasar reddening, as it is for only two of the five known OH absorbers.¹⁵ As is the case for the remaining three of the known systems, the absorption (and thus the cause of the reddening) could be occurring anywhere between us and the emission redshift of the quasar. Unfortunately, full range spectral scans are not feasible towards most sources with current instruments and, over the ranges which are scanned, there is a trade-off between the redshift space that can be covered and the depth of the search. This is our motivation for searching for molecular absorption within the host galaxy. Spectral scans have, however, been attempted (Murphy et al. 2003; Curran et al. 2005), with 0500 + 019 being one of the targets common to ours. We summarize the results in Table 3, from which we see that <30 per cent of the

¹⁵ As well as a possible detection towards 1107–187, which at $z = 0.48909$ (Curran et al. 2011a), is not covered by the 76.88–77.12 GHz ($0.4947 < z_{\text{CO}} < 0.4994$) range observed here (Fig. 2). 0213–026, 1504–166 and 1706 + 006 are undetected in 21 cm (Curran et al. 2011a), with the remainder of the sample as yet unsearched (see tables 1 and 2 of Curran & Whiting 2010).

redshift space towards 0500 + 019 has been scanned for HCO⁺ and only 12 per cent for CO, with some overlap in these ranges. We therefore cannot rule out that the cause of the reddening may be at some other redshift towards 0500 + 019 and indeed for the rest of the sample.

There is also the possibility that, even if the reddening (and hence any absorption) is located in the host, it would only be detected if the optical redshift is known precisely enough to ensure that the observed band covers the correct redshift range. The optical spectra of these quasars have spectral resolutions of $\approx 5\text{--}8 \text{ \AA}$, which corresponds to a few hundred km s^{-1} , which is close to our observed bandwidths (Fig. 2). However, most of the quasars observed here have strong narrow emission lines, which constrain the redshift to better than $\sim 10^{-4}$ and all are quoted to at least the third decimal place, although uncertainties are usually not given (Drinkwater et al. 1997). Referring to the ranges covered by our observed bands (Table 1), we see that offsets of $\Delta z \approx \pm 0.002$ (at low redshifts) to $\approx \pm 0.01$ (at high redshifts) are covered, thus making it unlikely that our observations are generally tuned to the wrong frequency.

4.3 Conditions within the host

Above we suggest the possibility that molecular absorption is not detected since the reddening of the quasar light may not necessarily be occurring close to the redshift of the background quasar. Over and above this, there is the possibility that a large column of absorbing molecular gas *cannot* be located in the host galaxy on the basis that there is a low fraction of cool neutral gas in the hosts of quasars and radio galaxies with ultraviolet luminosities of $L_{\text{UV}} \gtrsim 10^{23} \text{ W Hz}^{-1}$ (Curran et al. 2008). Whether this is due to excitation of the gas or these luminosities selecting gas-poor ellipticals (or indeed whether these two possibilities are interrelated, Curran & Whiting 2010), this appears to be the case for *all* redshifted ($z_{\text{em}} \gtrsim 0.1$) H I 21-cm absorption searches.

In order to investigate whether this could affect our sample, we use the photometry of the searched sources (Table 4) to derive the UV luminosities (as per Curran et al. 2008). Showing these in

Table 4. The magnitudes and calculated $\lambda \approx 1216 \text{ \AA}$ luminosities (W Hz^{-1}) of the quasars and radio galaxies searched in millimetre-wave absorption. The bottom panel lists the two known associated absorbers.

Quasar	z_{em}	Molecules	Ref.	B	V	K	Refs	$\log_{10}L_{\text{UV}}$
4C + 40.01	0.255	CO, HCO ⁺	W96	17.89	17.67	14.87	Z04, S06	22.34
PKS 0113 – 118	0.672	CO, HCO ⁺	D96	18.27	17.95	14.37	Z04	23.11
PKS 0213 – 026	1.178	CO, HCO ⁺	C11	21.33	20.82	15.17	F00	22.12
(HB89) 0234 + 285	1.213	CO	W95	19.20	18.35	13.33	A09, S06	23.37
PKS 0335 – 122	3.442	HCN	D96	21.02	20.11	17.51	E05, H01	23.92
(HB89) 0422 + 004	0.310	CO, HCO ⁺ , HCN	D96	13.89	14.12	11.31	F04	24.55
PKS 0434 – 188	2.702	HCO ⁺ , HCN	C08	19.25	–	16.24	E05	24.14
PKS 0438 – 436	2.852	CO	D96	20.74	19.91	16.09	B04, E05	23.77
PKS 0446 + 11	1.207	CO	W96	21.43	20.36	15.37	A09, S06	22.17
PKS 0454 + 06	0.405	CO	C11	19.38	18.74	14.42	F00	21.57
PKS 0500 + 019	0.58457	HCO ⁺	C11	22.50	21.35	15.6	D97, C03, S96b	20.38
PKS 0521 – 365	0.0552	HCO ⁺	D96	15.60	14.60	11.33	H07, S06	21.96
PKS 0528 + 134	2.065	CO	W95	20.09	20.00	15.06	Z04, G00	23.51
(HB89) 0537 – 441	0.894	CO, HCO ⁺ , HCN, CS	D96	17.93	17.34	13.02	F00	23.28
PKS 0601 – 17	2.711	HCO ⁺ , HCN	C08	20.45	–	–	H01	23.66
CGRaBS J0650 + 6001	0.455	CO	W96	20.85	–	14.63	Z04, S06	21.03
PKS 0727 – 115	1.591	CO	M03	21.13	20.07	14.52	A09, C03	22.42
(HB89) 0735 + 178	0.424	CO	W95	16.30	15.68	13.03	A09, S06	23.17
PKS 0823-223	0.9103	HCO ⁺	W96	–	16.11	12.34	F93	23.51
Hydra A	0.0538	CO, HCO ⁺	D96	13.90	12.87	10.90	V91, C03	23.89
(HB89) 0954 + 658	0.368	CO, HCO ⁺	W96	17.18	16.80	12.43	P04, S06	22.92
PKS 1026 – 084	4.276	CO	C08	21.07	–	–	H01	24.31
PKS 1107 – 187	0.497	CO	C11	22.44	21.10	15.95	F00	19.16
FTMJ1341 + 3301	1.720	HCO ⁺	C11	23.39	21.68	14.49	A09, G07	22.36
SBS 1347 + 539B	0.978	HCO ⁺	W96	17.95	17.52	15.07	A09, S06	23.72
(HB89) 1418 + 546	0.152	CO	W96	16.25	15.60	11.43	A09, S06	22.18
PKS 1430 – 155	1.573	CO	C11	22.50	23.24	17.50	D97, F00	21.79
3C 309.1	0.905	CO	W96	16.80	16.57	14.72	Z04, S06	24.27
PKS 1504 – 167	0.876	HCO ⁺	C11	20.28	19.75	14.01	F00	22.36
PKS 1548 + 056	1.422	CO	D96	19.37	18.65	14.30	F00	23.21
PKS 1555 + 001	1.77	CO, HCO ⁺	D96	20.34	19.95	16.24	F00	23.33
PKS 1622 – 253	0.786	HCO ⁺	W96	–	20.6	14.86	d94, S06	22.12
PKS 1622 – 29	0.815	HCO ⁺	W96	–	18.38	14.15	R02, S06	22.83
PKS 1725 + 044	0.296	CO, HCO ⁺	D96	17.92	17.46	14.13	F00	22.06
(HB89) 1749 + 096	0.322	CO, HCO ⁺	W96	17.98	17.39	12.00	O09, S06	21.87
(HB89) 1823 + 568	0.664	CO, HCO ⁺	W96	17.41	17.02	13.84	Z04, S06	23.18
Cygnus A	0.0561	CO, HCO ⁺	D96	17.04	15.52	10.28	V91, C03	20.78
CGRaB J2022 + 6136	0.228	HCO ⁺	W96	19.55	17.97	14.28	Z04, S06	20.19
(HB89) 2200 + 420	0.688	CO, HCO ⁺	W96	13.25	13.32	10.49	F04, S06	25.34
PKS 2223 – 052	1.404	CO	D96	18.59	18.33	14.69	F00	23.69
3C 454.3	0.859	HCO ⁺	W95	16.03	16.19	13.06	Z04, S06	24.11
PKS 2329 – 162	1.155	CO	D96	20.72	–	16.58	H01, W83	22.72
PKS 2337 – 334	1.802	HCO ⁺	C11	22.93	21.89	16.39	F00	22.05
PKS 1413 + 135	0.246710	CO, HCO ⁺ , HCN, HNC	W97	21.37	19.74	14.93	A09, S06	19.41
B3 1504 + 377	0.67150	CO, HCO ⁺ , HCN, HNC	W96	23.24	21.82	16.10	A09, S96a	19.81

Molecular search references: D96, Drinkwater et al. (1996); W95, Wiklind & Combes (1995); W96, Wiklind & Combes (1996b); W97, Wiklind & Combes (1997); M03, Murphy et al. (2003); C08, Curran et al. (2008); C11, this paper.

Photometry references: W83, Wright, Ables & Allen (1983); F93, Falomo et al. (1993); d94, di Serego-Alighieri et al. (1994); S96a, Stickel et al. (1996a); S96b, Stickel et al. (1996b); D97, Drinkwater et al. (1997); F00, Francis et al. (2000); G00, Ghosh et al. (2000); E01, Ellison et al. (2001); H01, SuperCOSMOS Sky Survey (Hambly et al. 2001); R02, Romero et al. (2002); C03, Cody & Braun (2003); B04, Brocksopp et al. (2004); F04, Fiorucci, Ciprini & Tosti (2004); P04, Papadakis et al. (2004); Z04, Zacharias et al. (2004); E05, Ellison, Hall & Lira (2005); S06, 2MASS (Skrutskie et al. 2006); A09, SDSS DR7 (Abazajian et al. 2009); O09, Ojha et al. (2009); FPC, P. Francis (private communication).

Fig. 6, we see the expected increase in luminosity with redshift and note that our selection of the reddest PHFS sources (Section 2.1) means that nearly all of our targets lie below $L_{\text{UV}} = 10^{23} \text{ W Hz}^{-1}$ (left-hand panel). Since we are unlikely to detect molecular absorption in an environment not conducive to large columns of cool neutral gas, in the right-hand panel of Fig. 6 we show UV luminosity versus *colour depth*, which we define as the optical–near-infrared colour normalized by the depth of the search. As expected of the

column density–($V - K$) correlation (Fig. 4), this gives a vertical line with this quantity plotted as the abscissa¹⁶ and from this

¹⁶ Adding the three intervening absorbers gives a *colour depth* of 1.00 ± 0.02 for both N_{CO} and $1000 \times N_{\text{HCO}^+}$. The intervening absorbers are not shown in the plot as, although the ultraviolet luminosities can also be estimated, these are remote from the source.

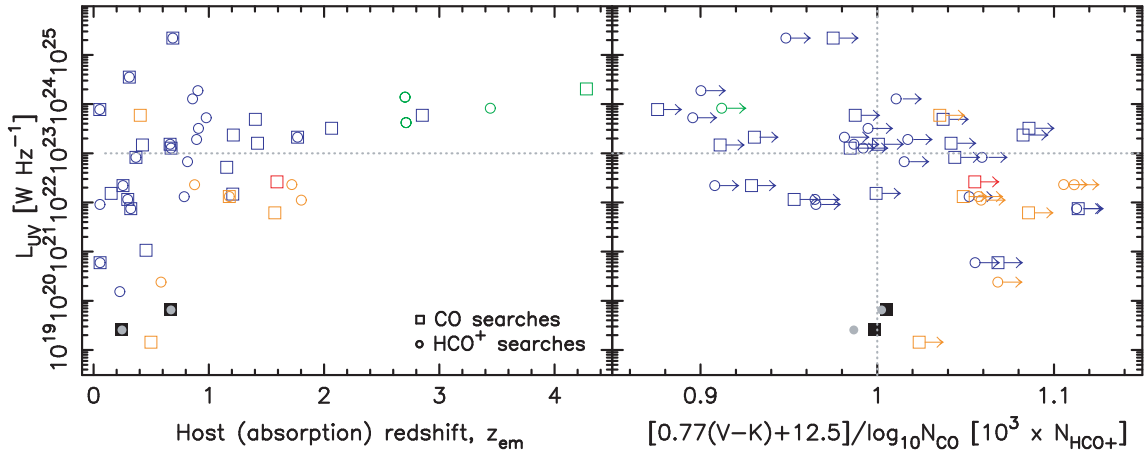


Figure 6. The ultraviolet ($\lambda \approx 1216 \text{ \AA}$) luminosity versus the redshift (left) and ‘colour depth’ [right] for the sources listed in Table 4. The *colour depth* is defined by the fit to the CO column density–colour correlation for the four known systems (Fig. 5, left), i.e. $[0.77(V - K) + 12.5]/\log_{10}N_{CO}$ and $0.77(V - K) + 12.5/\log_{10}(1000 \times N_{HCO^+})$, with the two known associated systems defining the vertical line at a value of 1.0. In the left-hand panel we show all of the sources searched, as V and K magnitudes are not required, nor is the recalculated 3σ rms noise required to be lower than the flux (as is not the case for the PKS 0422 + 004 searches nor HCO $^+$ in Hydra A, Drinkwater et al. 1996). Note that, after the $\times 1000$ normalization, the HCO $^+$ points (shown in grey for clarity) are located close to the CO points for the two known associated systems.

definition we see that 20 discrete sources (mostly from this work) have been searched sufficiently deeply, of which only 12 are located in the bottom-right quadrant defined by $L_{UV} \lesssim 10^{23} \text{ W Hz}^{-1}$ and a *colour depth* $\gtrsim 1$.

As expected, in Fig. 6 (right) there is an anticorrelation between UV luminosity and $V - K$ colour, since the former is derived from the observed frame optical photometry. As such, there is also the possibility that the calculated values of L_{UV} are influenced by the dust extinction towards the source. However, the fact that 21-cm absorption is never detected above a critical luminosity (or below a critical magnitude/dust extinction), as well as the correlation between the 21-cm absorption strength and $V - K$ colour (Curran & Whiting 2010), indicates that the extinction occurs within the host in the case of the 21-cm detections, which follow the expected 50 per cent detection rate for $L_{UV} \lesssim 10^{23} \text{ W Hz}^{-1}$ (Curran & Whiting 2010). Therefore, whether due to high intrinsic UV luminosities or a paucity of dust within the host galaxy, it remains that 21-cm absorption is not detected where $L_{UV} \gtrsim 10^{23} \text{ W Hz}^{-1}$ and where we do not detect 21-cm we do not expect to detect absorption by molecular gas.

Lastly, as well as a covering factor of $f \approx 1$, as per the four known systems, we have assumed an excitation temperature of $T_x \approx 10 \text{ K}$ (at $z = 0$) (Section 4.1). Since there is no apparent correlation between the optical–near-infrared colour and the excitation temperature for the four known systems (Table 2),¹⁷ we cannot estimate temperatures for any of the searched samples. If the gas were at higher excitation temperatures, being mostly observations of the lower rotational transitions (Table 1), the limits are less sensitive than quoted since a larger total column density would be required to give the same observed flux in these transitions. This has the effect of worsening the limits to the point where only two of the searched sources are (just) potentially detectable when $T_x \approx 100 \text{ K}$ (Fig. 7), although if the gas is diffuse, such excitation temperatures may not be attainable, even in the presence of high kinetic temperatures.

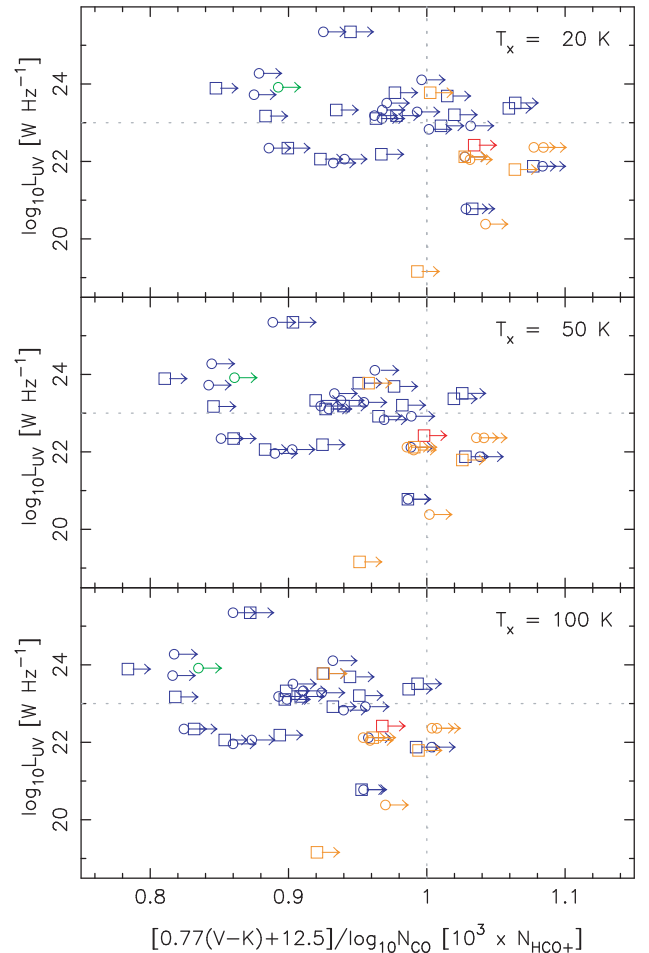


Figure 7. The *colour depth* distribution for various excitation temperatures.

5 SUMMARY

We have undertaken a survey of molecular absorption in the millimetre-band at a high redshift. Like all previous surveys (since

¹⁷ For 1413 + 135, $V - K = 4.81$ and $T_x = 8 \text{ K}$, similar to the excitation temperature of 1830–211 with $V - K = 6.25$.

Wiklind & Combes 1995, 1996a,b, 1997), we have not detected millimetre-band spectral line absorption in any of the targets. In the case of absorption due to intervening sources, it has been established that the paucity of detections is due to the traditional optical selection of these objects, in which the redshift of the intervening object is usually known, biasing against the reddest, and thus dustiest, absorption complexes (Curran et al. 2006). We have therefore aimed to circumvent this bias by searching for molecular absorption within the hosts of particularly red objects but, like Drinkwater et al. (1996) who also targeted red sources [and type-2 active galactic nuclei (AGN)],¹⁸ we find no absorption.

A possible reason for some of the non-detections is that only 12 of the 40 objects searched are known to be located in the bottom-right quadrant of the ultraviolet luminosity–colour depth plot (Fig. 6, right), i.e. where $L_{UV} \lesssim 10^{23} \text{ W Hz}^{-1}$ and $[0.77(V - K) + 12.5]/\log_{10} N_{CO} \approx [0.77(V - K) + 12.5]/\log_{10}(1000 \times N_{HCO^+}) \gtrsim 1$. This suggests that only a dozen of the sources may be subject to an ultraviolet flux which permits the presence of cool neutral gas (Curran et al. 2008), while being ‘sufficiently red’ to indicate the presence of a large column of dust along the sightline to the quasar (Curran et al. 2006). Based on these observations, we draw the following conclusions.

(i) For these, the reddening could be occurring anywhere along the line of sight, and not necessarily in the host galaxy, as is the case for three of the five known OH absorbers (four of which make up all the known redshifted millimetre-band absorbers). The only reason we chose to observe the emission redshift is that it gives a frequency to which to tune the receiver – Murphy et al. (2003) and Curran et al. (2005) previously attempted millimetre-wave spectral scans towards very dim objects, but the redshift range scanned is a trade-off with the time spent on each frequency, resulting in poor optical depth limits over what were limited redshift ranges in only a few sources.

(ii) This fifth absorber, which was detected in OH but not in HCO^+ , may be the result of lower millimetre-wave covering factors in comparison to those at decimetre wavelengths (Curran et al. 2007). This may be analogous to the effect seen in the optically selected DLAs (Section 1), where, due to the steeper cosmological evolution in the heavy element abundance in the H_2 -bearing DLAs, Curran et al. (2004c) suggest that these constitute a more homogeneous class of objects than the general population DLA (Prochaska et al. 2003). That is, H_2 absorption may only be observed in a limited subset of possible sightlines, and Zwaan & Prochaska (2006) suggest that a distinction could arise from the much smaller cross-section of the molecular gas, located in small and dense regions (e.g. Liszt & Lucas 1996), in comparison to that of the atomic gas. This means that only a narrow sightline will occult the quasar, although the DLA may be apparent through the more widespread 21-cm absorption.

(iii) As with covering factor effects, if the excitation temperature of the putative absorbing gas is higher than the assumed $T_x = 10 \text{ K}$ (at $z = 0$), the column density limits are poorer than those calculated here. When large enough ($T_x \gtrsim 100 \text{ K}$), none of these searches, mostly of the lower rotational transitions, were sensitive enough to detect CO or HCO^+ absorption in these sources, although the absorbing medium may be too diffuse to reach such temperatures through collisional excitation.

¹⁸ Although as Curran & Whiting (2010) have shown, the bulk cool neutral gas (as traced by $H\text{I}$ 21-cm absorption) is not located in the obscuring torus, invoked by unified schemes of active galactic nuclei.

Drinkwater et al. (1996) accounted for their non-detections by suggesting that the extinction may be occurring without the host galaxy or that the X-ray flux from the AGN may be photodissociating the molecules. These possibilities are similar to the points made above, although by quantifying these via the findings of Curran et al. (2006, 2008), we find that not all of the targets of Drinkwater et al. (1996) are sufficiently faint and reddened to have been detected, no matter the location of the obscuring material. Therefore, the key to finding new redshifted molecular absorbers in the millimetre-band is through the selection of the faintest optical objects (giving $L_{UV} \lesssim 10^{23} \text{ W Hz}^{-1}$) and performing spectral scans towards these to the colour depth limits of $\gtrsim 1$, as defined by the column densities and colours of the four known absorbers. In order to also circumvent the covering factor effect, pilot searches for OH in the decimetre band could be undertaken, with the low rest frequency (1667 MHz) allowing a full spectral scan in only four separate tunings with the Square Kilometre Array (Curran et al. 2004a).

ACKNOWLEDGMENTS

We would like to thank A. Weiss for assisting with the IRAM observations, as well as Shigeru Takahashi, Jun Maekawa and Hiroki Ashizawa of the Nobeyama Radio Observatory for their assistance in installing NEWSTAR and the data retrieval. MTM thanks the STFC for an Advanced Fellowship and the Australian Research Council for a QEII Research Fellowship (DP0877998).

We acknowledge financial support from the Access to Major Research Facilities Programme which is a component of the International Science Linkages Programme established under the Australian Government’s innovation statement, Backing Australia’s Ability.

This research has made use of the NASA/IPAC Extragalactic Data base (NED) which is operated by the Jet Propulsion Laboratory, California Institute of Technology, under contract with the National Aeronautics and Space Administration. This research has also made use of NASA’s Astrophysics Data System Bibliographic Services and ASURV Rev 1.2 (Lavalley, Isobe & Feigelson 1992), which implements the methods presented in Isobe et al. (1986).

Funding for the Sloan Digital Sky Survey (SDSS) and SDSS-II has been provided by the Alfred P. Sloan Foundation, the Participating Institutions, the National Science Foundation, the US Department of Energy, the National Aeronautics and Space Administration, the Japanese Monbukagakusho, the Max Planck Society, and the Higher Education Funding Council for England. The SDSS web site is <http://www.sdss.org/>.

REFERENCES

- Abazajian K. N. et al., 2009, *ApJS*, 182, 543
- Becker R. H., White R. L., Helfand D. J., 1995, *ApJ*, 450, 559
- Brockopp C., Puchnarewicz E. M., Mason K. O., Córdoba F. A., Pridhorsky W. C., 2004, *MNRAS*, 349, 687
- Carilli C. L., Perlman E. S., Stocke J. T., 1992, *ApJ*, 400, L13
- Carilli C. L., Rupen M. P., Yanny B., 1993, *ApJ*, 412, L59
- Carilli C. L., Menten K. M., Reid M. J., Rupen M. P., Yun M. S., 1998, *ApJ*, 494, 175
- Chandra S., Kegel W. H., Roy R. J. L., Hertenstein T., 1995, *A&AS*, 114, 175
- Chandra S., Maheshwari V. U., Sharma A. K., 1996, *A&AS*, 117, 557
- Chengalur J. N., de Bruyn A. G., Narasimha D., 1999, *A&A*, 343, L79
- Cody A. M., Braun R., 2003, *A&A*, 400, 871
- Curran S. J., Whiting M. T., 2010, *ApJ*, 712, 303

- Curran S. J., Kanekar N., Darling J. K., 2004a, *New Astron. Rev.*, 48, 1095
- Curran S. J., Murphy M. T., Pihlström Y. M., Webb J. K., Bolatto A. D., Bower G. C., 2004b, *MNRAS*, 352, 563
- Curran S. J., Webb J. K., Murphy M. T., Carswell R. F., 2004c, *MNRAS*, 351, L24
- Curran S. J., Webb J. K., Murphy M. T., Kuno N., 2005, in Engvold O., ed., *Highlights of Astronomy*, Vol. 13. Astron. Soc. Pac., San Francisco, p. 845
- Curran S. J., Whiting M., Murphy M. T., Webb J. K., Longmore S. N., Pihlström Y. M., Athreya R., Blake C., 2006, *MNRAS*, 371, 431
- Curran S. J., Darling J. K., Bolatto A. D., Whiting M. T., Bignell C., Webb J. K., 2007, *MNRAS*, 382, L11
- Curran S. J., Whiting M. T., Wiklind T., Webb J. K., Murphy M. T., Purcell C. R., 2008, *MNRAS*, 391, 765
- Curran S. J. et al., 2011a, *MNRAS*, 413, 1165
- Curran S. J., Whiting M. T., Tanna A., Bignell C., Webb J. K., 2011b, *MNRAS*, 413, L86
- di Serego-Alighieri S., Danziger I. J., Morganti R., Tadhunter C. N., 1994, *MNRAS*, 269, 998
- Drinkwater M. J., Combes F., Wiklind T., 1996, *A&A*, 312, 771
- Drinkwater M. J. et al., 1997, *MNRAS*, 284, 85
- Ellison S. L., Yan L., Hook I. M., Pettini M., Wall J. V., Shaver P., 2001, *A&A*, 379, 393
- Ellison S. L., Hall P. B., Lira P., 2005, *AJ*, 130, 1345
- Falomo R., Bersanelli M., Bouchet P., Tanzi E. G., 1993, *AJ*, 106, 11
- Fiorucci M., Ciprini S., Tosti G., 2004, *A&A*, 419, 25
- Francis P. J., Whiting M. T., Webster R. L., 2000, *Publ. Astron. Soc. Australia*, 17, 56
- Fukugita M., Ichikawa T., Gunn J. E., Doi M., Shimasaku K., Schneider D. P., 1996, *AJ*, 111, 1748
- Ghosh K. K., Ramsey B. D., Sadun A. C., Soundararajaperumal S., 2000, *ApJS*, 127, 11
- Glikman E., Gregg M. D., Lacy M., Helfand D. J., Becker R. H., White R. L., 2004, *ApJ*, 607, 60
- Hambly N. et al., 2001, *MNRAS*, 326, 1279
- Isobe T., Feigelson E., Nelson P., 1986, *ApJ*, 306, 490
- Jorgenson R. A., Wolfe A. M., Prochaska J. X., Carswell R. F., 2009, *ApJ*, 704, 247
- Kanekar N. et al., 2005, *Phys. Rev. Lett.*, 95, 261301
- Lavalley M. P., Isobe T., Feigelson E. D., 1992, *BAAS*, 24, 839
- Liszt H., Lucas R., 1996, *A&A*, 314, 917
- Murphy M. T., Curran S. J., Webb J. K., 2003, *MNRAS*, 342, 830
- Noterdaeme P., Ledoux C., Petitjean P., Srianand R., 2008, *A&A*, 481, 327
- Ojha R., Zacharias N., Hennessy G. S., Gaume R. A., Johnston K. J., 2009, *AJ*, 138, 845
- Papadakis I. E., Samaritakis V., Boumis P., Papamastorakis J., 2004, *A&A*, 426, 437
- Pickett H. M., Poynter R. L., Cohen E. A., Delitsky M. L., Pearson J. C., Müller H. S. P., 1998, *J. Quantitative Spectrosc. Radiative Transfer*, 60, 883
- Prochaska J. X., Gawiser E., Wolfe A. M., Castro S., Djorgovski S. G., 2003, *ApJ*, 595, L9
- Prochaska J. X., Herbert-Fort S., Wolfe A. M., 2005, *ApJ*, 635, 123
- Romero G. E., Cellone S. A., Combi J. A., Andruchow I., 2002, *A&A*, 390, 431
- Schneider D. P. et al., 2007, *AJ*, 134, 102
- Skrutskie M. F., Cutri R. M., Stiening R., Weinberg M. D., Schneider S., Carpenter J. M., Beichman C., Capps R. M., 2006, *AJ*, 131, 1163
- Srianand R., Noterdaeme P., Ledoux C., Petitjean P., 2008, *A&A*, 482, L39
- Srianand R., Gupta N., Petitjean P., Noterdaeme P., Ledoux C., 2010, *MNRAS*, 405, 1888
- Stickel M., Rieke G. H., Kühr H., Rieke M. J., 1996a, *ApJ*, 468, 556
- Stickel M., Rieke M. J., Rieke G. H., Kühr H., 1996b, *A&A*, 306, 49
- Wiklind T., Combes F., 1994, *A&A*, 286, L9
- Wiklind T., Combes F., 1995, *A&A*, 299, 382
- Wiklind T., Combes F., 1996a, *Nat*, 379, 139
- Wiklind T., Combes F., 1996b, *A&A*, 315, 86
- Wiklind T., Combes F., 1997, *A&A*, 328, 48
- Wiklind T., Combes F., 1998, *ApJ*, 500, 129
- Wright A., Otrupcek R., 1990, *Parkes Catalogue*. Australia Telescope National Facility
- Wright A. E., Ables J. G., Allen D. A., 1983, *MNRAS*, 205, 793
- Zacharias N., Monet D. G., Levine S. E., Urban S. E., Gaume R., Wycoff G. L., 2004, *BAAS*, 36, 1418
- Zwaan M. A., Prochaska J. X., 2006, *ApJ*, 643, 675

This paper has been typeset from a $\text{\TeX}/\text{\LaTeX}$ file prepared by the author.